

Charge dynamics in magnetically disordered Mott insulators

Philip Bleicker,^{1,*} Dag-Björn Hering,^{1,†} and Götz S. Uhrig^{1,‡}
¹*Lehrstuhl für Theoretische Physik I, Technische Universität Dortmund,
Otto-Hahn-Straße 4, 44221 Dortmund, Germany*
(Dated: April 21, 2021)

With the aid of both a semi-analytical and a numerically exact method we investigate the charge dynamics in the vicinity of half-filling in the one- and two-dimensional t - J model derived from a Fermi-Hubbard model in the limit of large interaction U and hence small exchange coupling J . The spin degrees of freedom are taken to be disordered. So we consider the limit $0 < J \ll T \ll W$ where W is the band width. We focus on evaluating the spectral density of a single hole excitation and the charge gap which separates the upper and the lower Hubbard band. One of the key findings is the evidence for the absence of sharp edges of the Hubbard band, instead Gaussian tails appear.

I. INTRODUCTION

Strongly correlated fermionic systems and Mott-Hubbard physics in particular continue to represent a great challenge to theoretical treatments in spite of many decades of research [1]. Even rather clear physical questions cannot be answered in a straightforward manner. A prominent example is the motion of a single hole in a Mott insulator. This issue has attracted a lot of interest early after the discovery of high-temperature superconductivity because it was noted that the hopping hole scrambles the antiferromagnetic background which can act as attractive force between two holes if the second one heals the misalignments caused by the first hole [2]. The motion of holes in ordered antiferromagnets continues to be a topic of current research [3], nowadays extended also to non-equilibrium situations [4].

Equally, the hole motion in a *disordered* spin background is a highly non-trivial issue. At first glance, one may think that there is no order to be scrambled such that the hole can move as freely as it does without any interaction so that the single particle Mott gap Δ is given by $(W - U)/2$ where W is the band width and U the local Hubbard repulsion. This expectation, however, is only correct in the extreme limit $U \rightarrow \infty$ and for hole motion on self-retracing paths, for instance in one dimension (1D) [5–7]. For finite values of U in a Hubbard model even the infinite-dimensional case yields a non-trivial value for the opening of the Mott gap computed to lie between $U_c \approx 1.11W$ [8, 9] and $U_c \approx 1.19W$ [10–15]. Note that in the considered paramagnetic infinite-dimensional case the spin background is indeed completely disordered without spin-spin correlations between different sites.

In 1D, the Bethe ansatz allows for an exact treatment [16] showing a Mott insulator at half-filling and zero temperature for infinitesimal interaction U . But it is also possible to consider a completely disordered spin background [17] corresponding to the situation where $J \ll$

$T \ll U \approx W$. Here, J is the nearest-neighbor (NN) anti-ferromagnetic exchange coupling taking the value $4t_0^2/U$ in leading order in the NN hopping t_0 [18–23] and W is the band width. Under this assumption, a Mott transition is identified to occur at $U_c = \sqrt{3}W/2 \approx 0.866W$. This finding provides an important benchmark. All these results illustrate that the hole motion is influenced by non-trivial quantum effects even for disordered spin backgrounds.

The aim of the present article is to study the hole motion in one and two dimensions (2D), i.e., along a chain and on a square lattice. The former case serves both as a benchmark and, due to its lower coordination number, as a system in which a larger number of processes with a larger spread is numerically accessible than in lattices with higher coordination numbers. This facilitates an in-depth spectral analysis and, in particular, the analysis of the typically difficult-to-access edges of the excitation spectrum. The latter case of a two-dimensional square lattice actually represents the most interesting case in view of experimental realizations in solid state systems or in cold atom setups. We consider the t - J model which is derived from the Hubbard model [18–24]. We stress that the mapping from the Hubbard model to the t - J model is not restricted to the magnetic exchange couplings, but naturally extends to the charge degrees of freedom, i.e., to hopping terms, hole-hole interactions, and correlated hopping processes. This applies to the chain [5] and to the square lattice [24, 25] at half-filling, but also in the vicinity of half-filling, i.e., for finite doping [26].

We proceed in two steps. First, we consider very large U , i.e., we omit all terms of order t_0^2/U and only keep terms of order U and t_0 . Second, we include the terms of order t_0^2/U to study to which extent they induce changes in the spectral densities including the character of the band edges. Such changes are expected, for instance the critical U deviates from W in the estimate $U_c \approx 1.10W$ obtained by Reischl et al. [25] for the square lattice.

A semi-analytic and a numeric approach are employed. The first, semi-analytic, approach relies on iterated equations of motion (iEoM) in the Heisenberg picture. The set of tracked operators is enlarged iteratively by commuting with the Hamiltonian, i.e. by applying the Liouville

* philip.bleicker@tu-dortmund.de

† dag.hering@tu-dortmund.de

‡ goetz.uhrig@tu-dortmund.de

superoperator. This Liouvillian acts on operators like a Hamiltonian acts on states [27, 28] yielding a Hermitian, oscillatory dynamics. The dominant part of the Liouvillian is the commutation with the hopping projected in such a way that no double occupancies are created or annihilated. Thus, the semi-analytic approach amounts up to a systematic expansion in the hopping element, that means in $x := t_0/U$. The second, numeric, approach tracks the hole motion in time on finite clusters with periodic boundary conditions in 1D and 2D by Chebyshev polynomial expansion [29–31].

This article is structured in the following way: In Sec. II, the Hubbard model and its simplification in the limit of strong interaction is explained briefly. Sec. III outlines the concepts and algorithms used to access the time-evolution of observables and to gain insight into the metal-insulator phase. Sec. IV provides data in the time domain comparing results from the two approaches used and illustrates how band edges are determined. In Sec. V and Sec. VI we discuss the results for the t - J model on the one-dimensional chain and on the two-dimensional square lattice, respectively. Summary and outlook are given in Sec. VII.

II. INITIAL MODEL

The Fermi-Hubbard model is one of the prime examples and archetypical models for strongly interacting electrons on a lattice and combines tight-binding electrons with a strongly screened Coulomb interaction [32–34]. In the following, we restrict our considerations to the one-band model in the vicinity of half-filling such that the Hamiltonian takes the form

$$H = H_0 + H_{\text{int}} \quad (1a)$$

$$H_0 = t_0 \sum_{\langle i,j \rangle, \sigma} (f_{i\sigma}^\dagger f_{j\sigma} + \text{h.c.}) \quad (1b)$$

$$H_{\text{int}} = U \sum_i \left(\hat{n}_{i\uparrow} - \frac{1}{2} \right) \left(\hat{n}_{i\downarrow} - \frac{1}{2} \right). \quad (1c)$$

Here, $f_{i\sigma}^\dagger$ ($f_{i\sigma}$) are the creation (annihilation) operators at site i for a fermion of spin σ and $\hat{n}_{i\sigma}$ is the corresponding number operator, t_0 denotes the real hopping matrix element between the sites i and j and $U > 0$ is the on-site interaction. As denoted in (1c), $U/2$ represents the energy cost if an electron is added inducing a double occupancy (DO) of two electrons at one site or, if a hole is added, inducing a double occupancy of holes at one site, i.e., creating an empty site. The kinetic energy H_0 is diagonal in momentum space such that all quasi-particles obey the dispersion relation

$$\varepsilon_{\mathbf{k}} := 2t \sum_{i=1}^d \cos(\mathbf{k}\mathbf{a}_i) \quad (2)$$

with \mathbf{a}_i denoting primitive translation vectors spanning the underlying Bravais lattice. The model is particle-hole

symmetric on bipartite lattices such as the 1D chain or the 2D square lattice.

A. Charge gap

The introduction of a large enough on-site interaction $U > 0$ in the Hubbard model splits the local density-of-states $\rho(E)$ into a lower (LHB) and an upper Hubbard band (UHB) as shown in Fig. 1.

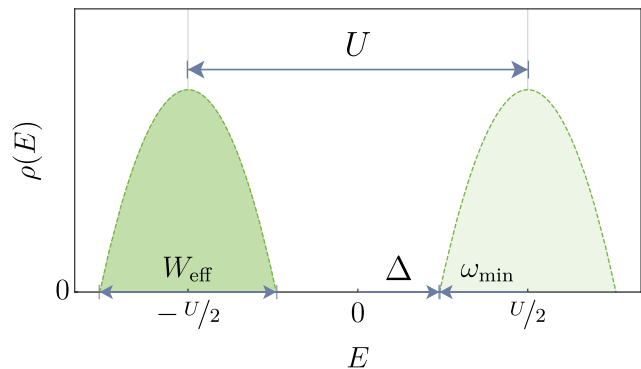


FIG. 1. For a large enough $U > 0$, the local density of states $\rho(E)$ splits into a lower and an upper Hubbard band at half-filling. Each band has the effective band width W_{eff} . The LHB is completely filled, the UHB is empty. Charge excitations take the form of DOs of electron or hole character with a minimum excitation energy of the gap Δ . Decreasing the on-site interaction reduces the gap until it closes at the critical interaction U_c .

Except for special cases, i.e., for specific lattices, cf. Introduction I, it remains an open question how the charge gap Δ behaves upon diminishing interaction strengths, for instance at which critical interaction strengths U_c the gap finally closes signalling the instability of the Mott insulator.

In this context, the 1D model plays a special role due to its integrability. It can be solved exactly by means of thermodynamic Bethe ansatz equations [16] at any temperature, but also under the assumption of a disordered spin background and charge excitations at zero temperature [17]. Yet we are not aware that the spectral density of the Hubbard models has been determined exactly by Bethe ansatz. Another possibility at finite temperatures is to use time-dependent density matrix renormalization group computations which allows one to determine spectral properties as well [7]. Moreover, the complementary limit of a Bethe lattice with an infinitely large coordination number $z \rightarrow \infty$ can be treated by dynamic mean-field theory readily providing information on the local spectral densities [8–15]. Otherwise, statements regarding the dynamics of charge carriers are difficult to provide. We address this very question using two fundamentally different techniques in the remainder of the work.

B. Effective Model: t - J Model

In the limit of strong interaction, i.e., $x = t_0/U \ll 1$, the Hubbard model can be mapped to the t - J model and thereby simplify it based on perturbation theory in the small parameter x . We consider all linear U terms in zeroth order as well as the $xU = t_0$ term H_0 describing hopping in first order. Contributions of second order, i.e., especially magnetic superexchange $J \propto x^2U$, and contributions of even higher orders are neglected in the first step, but will be considered in a second step. First, we study a Hamiltonian of the general form

$$H_{\text{eff}} = H_{\text{int}} + H_0 + \mathcal{O}(x^2U). \quad (3)$$

A systematic approach to derive such an effective model is to resort to a continuous unitary transformation (CUT) [23, 25, 26, 35–38]. For the sake of completeness, we will briefly recall the concepts as presented in Ref. [25] here. For a CUT one conventionally starts with the flow equation [35] as given by

$$\frac{d}{d\ell} H(\ell) = [\eta(\ell), H(\ell)] \quad (4)$$

with a properly chosen antihermitian generator $\eta(\ell)$. Similar to the perturbative reasoning [18–22], the key idea is to eliminate processes which *change* the number of DOs so that the final effective Hamiltonian preserves the number of DOs. To this end, one can choose

$$\eta(\ell) = \left[\hat{D}, H(\ell) \right] \quad (5)$$

where $\hat{D} := \sum_i [n_{i,\uparrow}n_{i,\downarrow} + (1 - n_{i,\uparrow})(1 - n_{i,\downarrow})]$ counts the number of DOs, i.e., all sites occupied by either two particles or completely empty. We stress that the resulting generator is proportional to the ones with *sign* functions [25, 36, 37] due to the simplicity of \hat{D} . Governed by the flow equation (4) a transformation from the initial Hamiltonian $H(0) = H$ to the effective Hamiltonian

$$H_{\text{eff}} = \lim_{\ell \rightarrow \infty} H(\ell) \quad (6)$$

takes place. It is this effective Hamiltonian one is usually interested in. Obviously, it is necessary to restrict the number of contributing operator terms generated by the flow equation in a suitable manner. One possibility, employed in Refs. [25, 26], is to define a proper measure of locality: operator terms which are not sufficiently local are discarded. Since the non-locality of the Hubbard model is due to the hopping, this approach corresponds to an expansion in t_0 . This procedure eventually leads to a generalized t - J model at half-filling [25] and for moderate doping [26]. The leading order at half-filling is known also analytically [5, 6, 24].

Exploiting the assumption $0 < J \ll T \ll W$ where the temperature T is much larger than the typical magnetic coupling strength J we consider a completely disordered spin background. The charge carriers, however, behave

as if the system were essentially at vanishing absolute temperature $T \approx 0$. The effective hopping processes in the t - J model can be split in the following way

$$H_{0,\text{eff}} = T_0 + T'_0 + T'_{s,0} + T''_0 + T''_{s,0}. \quad (7)$$

For the sake of brevity, we will use the term t - J model in the following for the above hopping model even if the magnetic exchange is not present. The magnetic exchange interaction can easily be added to $H_{0,\text{eff}}$. We will come to this complete t - J model at a later stage of this article.

In Eq. (7) the term T_0 describes nearest-neighbor (NN) hopping from site i to j and vice-versa subjected to the restraint that DOs neither are added nor removed, i.e.,

$$T_0 = t_0 \sum_{\langle i,j \rangle, \sigma} \left[(1 - n_{i,\sigma}) c_{i,\bar{\sigma}}^\dagger c_{j,\bar{\sigma}} (1 - n_{j,\sigma}) + n_{i,\sigma} c_{i,\bar{\sigma}}^\dagger c_{j,\bar{\sigma}} n_{j,\sigma} + \text{h.c.} \right]. \quad (8)$$

Here and in the following, the notation of the sums means a one-time counting of each bond between the lattice sites i and j and $\bar{\sigma}$ denotes the opposite of the orientation σ . The generalization of such hopping to next-nearest neighbor (NNN) hopping processes, i.e., all processes between sites on the 2D square lattice which lie on adjacent *diagonal* positions, are denoted by

$$T'_0 = t' \sum_{\langle\langle i,j \rangle\rangle; \sigma} \left[(1 - n_{i,\sigma}) c_{i,\bar{\sigma}}^\dagger c_{j,\bar{\sigma}} (1 - n_{j,\sigma}) - n_{i,\sigma} c_{i,\bar{\sigma}}^\dagger c_{j,\bar{\sigma}} n_{j,\sigma} + \text{h.c.} \right]. \quad (9)$$

Likewise, hopping processes between third-nearest neighbor (3NN) sites, i.e., sites that lie in-line on one of the axes and are separated by two links, are described by the contributions of

$$T''_0 = t'' \sum_{\langle\langle\langle i,j \rangle\rangle\rangle; \sigma} \left[(1 - n_{i,\sigma}) c_{i,\bar{\sigma}}^\dagger c_{j,\bar{\sigma}} (1 - n_{j,\sigma}) - n_{i,\sigma} c_{i,\bar{\sigma}}^\dagger c_{j,\bar{\sigma}} n_{j,\sigma} + \text{h.c.} \right]. \quad (10)$$

In 1D, only the second type, i.e., the contribution T''_0 , exists because there are no diagonals so that the double-prime processes represent next-nearest neighbor hopping. Since this makes the nomenclature NN, NNN and 3NN ambiguous if 1D and 2D are considered both, we use the terms *prime* and *double-prime* hopping instead. In 2D, both exist; in 1D only the double-prime hopping.

Apart from these hopping processes further *spin-dependent* hops can occur in the effective model. Whenever charges hop from one site to another, e.g., from i to j , with a NN site k in between, spin-dependent hops of the form

$$T'_{s,0} = t'_s \sum_{\substack{\langle i,k,j \rangle \\ \alpha, \beta}} \left\{ [(1 - n_{i,\alpha}) c_{i,\alpha}^\dagger \sigma_{\alpha,\beta} c_{j,\beta} (1 - n_{j,\beta})] \cdot \mathbf{S}_k \right.$$

$$+ [n_{i,\alpha} c_{i,\alpha}^\dagger \sigma_{\alpha,\bar{\alpha}} c_{j,\bar{\beta}} n_{j,\beta}] \cdot \mathbf{S}_k + \text{h.c.}] \quad (11a)$$

$$T''_{s,0} = t''_s \sum_{\substack{\langle\langle i,k,j \rangle\rangle \\ \alpha,\beta}} \left\{ [(1 - n_{i,\alpha}) c_{i,\alpha}^\dagger \sigma_{\alpha,\bar{\alpha}} c_{j,\bar{\beta}} (1 - n_{j,\beta})] \cdot \mathbf{S}_k \right. \\ \left. + [n_{i,\alpha} c_{i,\alpha}^\dagger \sigma_{\alpha,\bar{\alpha}} c_{j,\bar{\beta}} n_{j,\beta}] \cdot \mathbf{S}_k + \text{h.c.}] \right\} \quad (11b)$$

occur. These processes not only involve the hopping of a fermion over a nearest-neighbor, but also its interaction with the spin of this nearest-neighbor. For instance, the spin of the hopping fermion may swap with the spin of the nearest-neighbor. Just like the hopping processes in (9) and (10), the spin-dependent processes (11) do not change the overall number of DOs. As before, in 1D only the double-prime processes exist because of the lack of diagonals. The leading orders of the contributions that emerge in this process may be determined analytically via perturbation-theoretical approaches [5, 24] or numerically by means of the above-discussed CUT [25].

In the following, we make use of the values derived analytically for 1D in Ref. [5] which read

$$t'' = -\frac{t_0^2}{2U} \quad (12a)$$

$$t''_s = \frac{t_0^2}{U}. \quad (12b)$$

A generalization of these contributions to the additional processes arising in 2D is easily possible. In 2D, there is exactly one shortest route from i to j which can generate a t'' contribution. For diagonal hopping, i.e., for t' , there are two shortest routes. A diagonal step on a square lattice can happen via first a horizontal step and then a vertical step or vice-versa. For spin-independent diagonal hopping, both routes contribute and hence we have a factor 2

$$t' = -\frac{t_0^2}{U}. \quad (13)$$

For spin-dependent processes the involved intermediate lattice site k distinguishes the two routes so that no doubling is needed

$$t'_s = \frac{t_0^2}{U}. \quad (14)$$

These leading contributions (13) and (14) generalized for 2D are consistent with the numerically determined contributions t' and t'_s of comparable studies, cf. Ref. [25]. They also agree with the 2D results in Ref. [24].

So far only the charge degrees of freedom are considered with $H_{0,\text{eff}}$. Next, we extend the model by the spin-spin interactions. This model is equivalent to what is called t - J model in the literature, except that we include the interaction term H_{int} to keep track of the energy shifts. The additional Heisenberg contribution reads

$$H_J = J \sum_{\langle i,j \rangle} \mathbf{S}_i \mathbf{S}_j = \frac{J}{2} \sum_{\langle i,j \rangle} \left(P_{ij} - \frac{1}{2} \right) \quad (15)$$

with $J = 4t_0^2/U$ so that the effective Hamiltonian becomes

$$H_{\text{eff}} = H_{0,\text{eff}} + H_J. \quad (16)$$

The alternative notation employing the permutation operator P_{ij} , which interchanges two spins on the lattice sites i and j is equivalent to the spin-spin exchange for $S = 1/2$. It is particularly useful in numerics where quantum mechanical states are represented by bit patterns.

Recalling the bandwidth $W = 2zt_0$ with the coordination number z of the lattice helps us to identify the physically relevant parameter choices. Inserting it into the leading contributions above, it is easy to identify relevant physical regimes. We focus on two parameter sets (A) and (B). The first is motivated from the application to cuprates where $J = t_0/3$ is a representative value. The second parameter set (B) is theoretically motivated. It represents roughly the boundary value $U = W$ up to which the mapping from the Fermi-Hubbard model to the t - J model is reasonable [25, 26]. For lower values of the interaction the assumption of split Hubbard bands is no longer justified. Case (B) is of particular interest because it represents the limiting case with maximum second-order terms in the t - J model. For ease of identification, we use the abbreviations (A) and (B) below to distinguish between these parameter sets. We emphasize that in case (B) different second order terms occur depending on the dimension d of the system. For instance, for the magnetic coupling we have

$$(A) \quad J = \frac{t_0}{3} \quad (17a)$$

$$(B) \quad J = \frac{t_0}{d}. \quad (17b)$$

III. METHODS

In this section, we present a brief overview over the methods used to calculate the quantities computed in this article. Importantly, we point out the strengths and shortcomings of the techniques used. In-depth derivations can be found in the references given.

The lower band edge of the Hubbard band of the hole is a key quantity. If it falls below $U/2$ the assumed Mott insulator is unstable. The determination of ω_{min} is achieved using two fundamentally different approaches. In the first approach using iterated equations of motion (iEoM), we obtain the energy spectrum of the system and consequently have direct access to the minimum energy ω_{min} of the lowest-lying excitation. In the second approach, we simulate the full dynamics of the hole-doped t - J model in a numerically exact manner by means of the Chebyshev expansion technique (CET) providing the spectral function of the initial hole excitation.

The two methods appear similar at first glance, but the crucial difference resides in the fact that the iEoM approach works in the Heisenberg picture addressing

operators while the Chebyshev expansion treats quantum states. The iEoM approach systematically truncates the underlying Hilbert space of operator monomials, but treats the thermodynamic limit of an infinite lattice. The CET considers the whole Hilbert space with exponentially increasing dimension for increasing system size. This requires to consider finite systems. For the iEoM approach, no simulation of the time dependence of the hole-doped t - J model up to a specific threshold time t_{\max} needs to be performed. Instead, the excitation spectrum can be deduced directly by diagonalization. We start by a dedicated analysis of iEoM in Sec. III A before the numerical approach of CET is presented in Sec. III B.

A. Iterated equations of motion

In order to deduce the full energy spectrum and the lower band edge in particular we resort to the iterated equations of motion approach [39–41], a brief summary of which is given in the first part of this section. The second part is dedicated to the necessary modifications of the method which warrant a unitary time evolution on the operator level [27, 28], and the third part describes the concrete application of the iEoM to the t - J model.

We start by considering an arbitrary operator in the Heisenberg picture

$$A(t) = \sum_i h_i(t) A_i. \quad (18)$$

Here, all time dependence is contained in the complex prefactors $h_i(t)$; the constant operators A_i from the Schrödinger picture form an operator basis. In the following, \hbar is set to unity for simplicity. The linear independence of the A_i is required since otherwise the above expansion (18) would not be unique. Without explicit time dependence of the Hamiltonian the Heisenberg equation of motion becomes

$$\frac{d}{dt} A(t) = i[H(t), A(t)] =: i\mathcal{L}(A(t)) \quad (19)$$

with the Liouville superoperator $\mathcal{L}(\cdot)$. Then, inserting Eq. (18) into (19) leads to

$$\frac{d}{dt} A(t) = i\mathcal{L}(A(t)) \quad (20a)$$

$$= i \sum_i h_i(t) \mathcal{L}(A_i). \quad (20b)$$

It is possible to expand all operators $\mathcal{L}(A_i)$ in the chosen basis $\{A_i\}$ by

$$\mathcal{L}(A_i) := \sum_j M_{ji} A_j \quad (21)$$

leading to the Liouvillian matrix \mathbf{M} , also called dynamic matrix. For a compact notation, it is advisable to combine the time dependent prefactors $h_i(t)$ to a vector $\mathbf{h}(t)$.

Its dynamics is given by

$$\frac{d}{dt} \mathbf{h}(t) = i\mathbf{M}\mathbf{h}(t). \quad (22)$$

For the computation of the Liouvillian matrix, it is convenient to use an orthonormal operator basis $\{A_i\}$ (ONOB) so that each matrix element can be computed directly by

$$M_{ji} = (A_j | \mathcal{L}(A_i)). \quad (23)$$

It has been previously shown [27, 28] that it is crucial to achieve Hermiticity of \mathbf{M} , i.e., preserving the property $M_{ji} = M_{ij}^*$ in order to obtain oscillatory solutions. Otherwise, exponentially increasing solutions are possible and will occur. They definitely do not reflect physical behavior. The Hermiticity of \mathbf{M} is tantamount to $\mathcal{L}(\cdot)$ being self-adjoint. To achieve this property, one has to use a suitable operator scalar product for two linear operators A and B defined on a locally finite-dimensional Hilbert space \mathcal{H} , i.e., $\dim(\mathcal{H}) < \infty$. An advantageous choice is the Frobenius scalar product

$$(A|B) := \mathcal{N} \text{Tr}(A^\dagger B) \text{ with } \mathcal{N} := \frac{1}{\text{Tr}(\mathbb{1})}. \quad (24)$$

The prerequisite of a locally finite-dimensional Hilbert space clearly holds for all spin systems and all fermionic systems such as the Fermi-Hubbard model or models like the t - J model with both spin and fermionic degrees of freedom. Bosonic degrees of freedom are excluded due to their locally infinite-dimensional Hilbert spaces.

Note that the scalar product (24) can also be interpreted physically since it equals the high-temperature limit $T \rightarrow \infty$ of the thermal expectation value

$$(A|B) = \lim_{T \rightarrow \infty} \langle A^\dagger B \rangle \quad (25a)$$

$$= \lim_{T \rightarrow \infty} \text{Tr}(\rho A^\dagger B) \quad (25b)$$

in the canonical ensemble for a density matrix $\rho = e^{-\beta H}/Z$ with the partition sum $Z = \text{Tr}(e^{-\beta H})$ and the inverse temperature $\beta \geq 0$. Using this very scalar product ensures that $\mathcal{L}(\cdot)$ is indeed self-adjoint and thus that the dynamic matrix is Hermitian. This stems from the invariance of the trace under cyclic permutations in (23), see Ref. [27] and especially Ref. [28].

Next, one has to choose an appropriate operator basis $\{A_i\}$ to describe the dynamics of a hole excitation in the half-filled t - J model. Generally, there are various techniques to do so by either resorting to the iterative approach of looping operators, cf., especially Refs. [40, 41], or by using a closed operator basis which has to be constructed *a priori* as was done in, e.g., Ref. [28]. The advantage of the first approach is that it considers more operators relevant to the actual dynamics while the advantage of the second approach is that it is simpler to ensure the orthonormality of the operator basis since it is constructed beforehand.

In the following, we present a mixed approach that combines the strengths of both techniques. We recall that for two bounded operators A_1 and A_2 acting on two different Hilbert spaces \mathcal{H}_1 and \mathcal{H}_2 the trace in the product space $\mathcal{H} = \mathcal{H}_1 \otimes \mathcal{H}_2$ can be split into two factors

$$\text{Tr}(A_1 A_2) = \text{Tr}_1(A_1) \text{Tr}_2(A_2), \quad (26)$$

where $\text{Tr}_m(\cdot)$ denotes the partial trace over \mathcal{H}_m . Hence, in the Hilbert space of an N -site lattice the trace of a product of operators acting on different sites can be factorized into a product of local traces in the four-dimensional local Hilbert space spanned by $\{|0\rangle, |\uparrow\rangle, |\downarrow\rangle, |\uparrow\downarrow\rangle\}$. This fact helps us to establish an unambiguous representation of operators. Each given operator can be decomposed into a product of operators acting on different sites where the 16 local operators listed in Table I form a local orthogonal basis. The operator $n^u = (n_\downarrow - 1/2)(n_\uparrow - 1/2)$ measures the deviation from half-filling at a given site: at half-filling $n^u = -1/4$ holds, in presence of a DO (electron or hole) $n^u = 1/4$ holds. Note that here site indices and the resulting normalization factors are omitted for brevity. We stress that the local operators in Table I are mutually orthogonal, but not normalized.

$\mathbb{1}$	n^u	$\sigma^+ = f_\uparrow^\dagger f_\downarrow$	$f_\downarrow f_\uparrow$
$n_\downarrow - 1/2$	$n_\uparrow - 1/2$	$\sigma^- = f_\downarrow^\dagger f_\uparrow$	$f_\downarrow^\dagger f_\uparrow^\dagger$
$\bar{d}_\downarrow^\dagger = f_\downarrow^\dagger f_\uparrow^\dagger f_\uparrow$	$\bar{d}_\uparrow^\dagger = f_\uparrow^\dagger f_\downarrow^\dagger f_\downarrow$	$\bar{h}_\downarrow^\dagger = f_\downarrow f_\uparrow f_\uparrow^\dagger$	$\bar{h}_\uparrow^\dagger = f_\uparrow f_\downarrow f_\downarrow^\dagger$
$\bar{d}_\downarrow = f_\downarrow f_\uparrow^\dagger f_\uparrow$	$\bar{d}_\uparrow = f_\uparrow f_\downarrow^\dagger f_\downarrow$	$\bar{h}_\downarrow = f_\downarrow^\dagger f_\uparrow^\dagger f_\uparrow$	$\bar{h}_\uparrow = f_\uparrow^\dagger f_\downarrow^\dagger f_\downarrow$

TABLE I. Operator basis for a four-dimensional local Hilbert space being orthogonal with respect to (24). The overbars indicate that the creation operators imply a certain projection compared to standard fermionic creation operators. As denoted, the operators are not normalized.

In order to describe the dynamics of a hole inserted into the disordered spin background we consider the time evolution of the operator $h_{i\uparrow}^\dagger(t)$. Initially, $h_{i\uparrow}^\dagger(t=0) = h_{i\uparrow}^\dagger$ holds so that the initial condition for the prefactors h_i in (18) reads

$$h_i(0) = \begin{cases} 1 & \text{if } i = 1 \\ 0 & \text{otherwise,} \end{cases} \quad (27)$$

setting $A_1 := h_{i\uparrow}^\dagger$. Starting from $h_{i\uparrow}^\dagger$ the operator basis $\{A_i\}$ is constructed by repeatedly applying the Liouville superoperator to the current basis operators, simplifying the results so that the local operators are one of 16 local operators in Table I. In this way, an operator of the basis is constructed as operator monomial, i.e., a product of the local operators on a certain subset of sites of the lattice. The monomials which are created for the first time by the current iteration extend the basis. The

total number of applications of $\mathcal{L}(\cdot)$ to the basis operators is called the order m of the iterative extension of the basis of monomials. We call one iteration of $\mathcal{L}(\cdot)$ a *loop*. This means, for instance, that three commutations of the Hamiltonian H yield the so called 3-loop basis. Generally, m iterations of $\mathcal{L}(\cdot)$ lead to the m -loop basis.

$\mathbb{1}$	$\sigma^z = n_\uparrow - n_\downarrow$	σ^+	σ^-
$\bar{d}_\downarrow^\dagger$	$\bar{h}_\downarrow^\dagger$	\bar{d}_\uparrow^\dagger	\bar{h}_\uparrow^\dagger

TABLE II. Reduced operator basis for the two-dimensional local Hilbert space. All pairs of operators are orthogonal with respect to (24), but the operators are not normalized.

Our aim is to capture the dynamics of a single hole, i.e., a DO of holes, or a single DO of particles at half-filling. The above procedure, however, generates operators which are effective on an increasing number of DOs. The corresponding monomials are relevant if larger levels of doping are considered. But for the particular goal here they are detrimental in two respects: (i) they represent a computational burden leading to unnecessarily large operator bases; (ii) they correspond to processes which cannot take place at half-filling leading to spurious eigenvalues of the dynamic matrix \mathbf{M} . The corresponding eigenvectors do not matter at half-filling. Hence, it is indicated to discard the monomials which are effective only for two or more DOs and we restrict the tracked operator monomials to those creating a single hole or a single DO. This means that in the relevant monomials there is only a single site with a hole/DO creation operator \bar{h}_σ^\dagger or \bar{d}_σ^\dagger . At all other sites, where the operator monomial has a non-trivial effect, only operators which conserve the number of DOs *and* which have a non-zero effect at half-filling appear. These are the operators of the upper row in Table II. The lower row in this table lists the operators which create the hole/DO at the one site of the operator monomial. Charge hopping processes can only occur at this particular site. It is sufficient that the normalization factor is calculated by the trace in the reduced half-filled Hilbert space, i.e., summing over the two local states $|\uparrow\rangle$ and $|\downarrow\rangle$ only.

For the iterative construction of the operator basis we apply the Liouvillean, corresponding to the commutation with H_{eff} , with or without the prime and double-prime terms recursively. The resulting operators are expanded in operator monomials of which only those are kept which create a DO at one site and elsewhere only consist of operators of the upper row in Table II. This reduces the computational effort considerably and provides the physically relevant dynamic matrix \mathbf{M} . The identity operator $\mathbb{1}$ does not need to be tracked. Once the operator basis of monomials is determined, the dynamic matrix \mathbf{M} is calculated using (23) and diagonalized leading to the desired set of eigenvalues ω_n and the corresponding eigenvectors \mathbf{v}_n .

Given the enormous size of the underlying Hilbert

space of operators, i.e., the enormous size of the dimension of \mathbf{M} , it is necessary to resort to efficient diagonalization techniques such as the Arnoldi iteration [42] which simplifies to the well-known Lanczos algorithm [43] in case of Hermitian matrices. Since the Hermiticity of \mathbf{M} is guaranteed by construction the Lanczos algorithm can be employed to compute the (reduced) f -dimensional Krylov space and the corresponding set of eigenvalues and eigenvectors. We denote these reduced sets by $\bar{\omega}_n$ and $\bar{\mathbf{v}}_n$, respectively. With the help of these sets the dynamics of the system can be expressed to very good accuracy as a linear combination according to

$$\mathbf{h}(t) = \sum_{n=1}^f \alpha_n e^{i\bar{\omega}_n t} \bar{\mathbf{v}}_n \quad (28)$$

with the coefficient set α_n chosen in such a way that the initial condition given by Eq. (27) is fulfilled. We varied the dimension f of the Krylov space to monitor if any changes in the results occur. We finally chose $f = 200$ from which on no changes can be discerned anymore. In particular, the minimum of $\bar{\omega}_n$ represents a very reliable estimate for the band edge. As long as $U/2 + \bar{\omega}_n > 0$, the Mott insulating phase is locally stable.

Since we consider a fully disordered spin background we do not deal with a pure state but with a mixed ensemble corresponding to the high-temperature limit of the canonical ensemble $\rho \propto e^{-\beta H}$, i.e., to the density matrix

$$\rho_0 \propto \mathbb{1}. \quad (29)$$

We insert a hole into it at time $t = 0$ using the respective creation operator $\bar{h}_{i\uparrow}^\dagger$. The dynamics of this charge excitation is described by the retarded Green's function

$$g(t) = -i \text{Tr} \left(\bar{h}_{i\uparrow}^\dagger(t) \bar{h}_{i\uparrow}^\dagger \rho_0 \right) \theta(t) \quad (30)$$

where $\theta(t)$ stands for the Heaviside function. No commutator appears because the corresponding term vanishes since no hole can be annihilated in the exactly half-filled state.

In the framework of the iEOMs the above retarded Green's function is found by inserting the operator expansion (18) into (30) twice, once for the creation and once for the annihilation operator leading to

$$g(t) = -i \left\langle \bar{h}_{i\uparrow}^\dagger(t) \bar{h}_{i\uparrow}^\dagger \right\rangle \theta(t) \quad (31a)$$

$$= -i \sum_{mn} h_m(t) h_n^*(0) \langle A_m A_n^\dagger \rangle \theta(t) \quad (31b)$$

$$= -i \sum_n |\alpha_n|^2 e^{i\bar{\omega}_n t} \theta(t). \quad (31c)$$

Note that $\langle A_m A_n^\dagger \rangle = \delta_{mn}$ holds since the corresponding operator basis A_m is orthonormal with respect to (24). The spectral density $A(\omega)$ can be obtained from

the Fourier transform $g(\omega)$ of (31c)

$$A(\omega) = -\frac{1}{\pi} \text{Im} g(\omega) \quad (32a)$$

$$= \sum_n |\alpha_n|^2 \delta(\omega - \bar{\omega}_n). \quad (32b)$$

As expected, the modulus squared of the coefficients α_n indicates the weight and hence the relative importance of the corresponding process for the hole dynamics.

A finite number of iterations, i.e., a finite order m , implies that only processes with a finite spatial spread in the infinite system are taken into account. This implies that only a finite number of eigenvalues ω_n occurs so that the spectral density (32a) is not continuous, but consists of discrete δ -spikes. This discreteness also results from the use of a finite-dimensional Krylov space in the Lanczos diagonalization. But this effect is straightforward to control because the Krylov dimension f can easily be increased by for instance, a factor 2. The finiteness, however, of the loop order m cannot be increased easily. In order to plot spectral densities and to compare them between different approaches, we broaden the δ -spikes artificially by Gaussians according to

$$A(\omega) = \sum_n \frac{|\alpha_n|^2}{\sqrt{2\pi}\sigma} \exp\left(-\frac{(\omega - \bar{\omega}_n)^2}{2\sigma^2}\right). \quad (33)$$

The artificial broadening σ has the unit of an energy, recall $\hbar = 1$, and its value will be discussed below.

B. Chebyshev expansion technique

As many numerical approaches, the CET needs a finite-dimensional Hilbert space so that only finite clusters can be dealt with. This calls for a suitably chosen complete set of orthonormal states $\{|i\rangle\}$ forming a basis of the Hilbert space \mathcal{H} for the Hamiltonian (7). In contrast to the previous section, we stress that CET works in the Schrödinger picture so that the states are the usual kets. To increase the overall performance we resort to an integer representations of the basis states. We exemplify this procedure in the following before discussing how to derive Green's functions from the Hamiltonian matrix. Consider a t - J model doped with a single hole where exactly one hole is inserted into a lattice of N sites. Then, the dimension of the Hilbert space is $\dim(\mathcal{H}) = N 2^{N-1}$ since the hole may occupy one of N sites while on all remaining sites the spins $1/2$ can point upwards or downwards. For notational simplicity, we artificially enlarge the basis size to $d = N 2^N$ states while keeping in mind that the spin orientation at the site occupied by the hole has no physical meaning. In this way, a real space basis of the binary form

$$|i\rangle = |i_{N-1} \dots i_0\rangle |h_{N-1} \dots h_0\rangle \quad (34)$$

can be constructed. Here, all spins can be either orientated upwards, i.e., $\uparrow \equiv 0$, or downwards, i.e., $\downarrow \equiv 1$, so

that the relation $i_j \in \{0, 1\}$ holds. The hole always occupies exactly one site $h_k = 1$ with all remaining sites being empty such that $h_j = 0 \forall j \neq k$. This allows for an easy and concise identification of a given basis state $|i\rangle$ by the integer representation $I \in 0, \dots, N 2^N - 1$ using

$$I = k 2^N + \sum_{j=0}^{N-1} i_j 2^j \quad (35)$$

where the last sum is equal to the integer value of the binary number given by the binary pattern of the spin orientations. As long as we do not consider the magnetic exchange H_J the dynamics in the t - J model *only* occurs at the hole position k . This facilitates the numerical task considerably. It is possible to construct the respective Hamiltonian matrix either on-the-fly by algorithms linear in the basis size or to keep a highly sparse copy of it.

In order to compute spectral densities with the CET, we determine the retarded Green's function $g(t)$ in a first step. The trace over the half-filled Hilbert space in (30) has to be taken which could strongly limit this approach. Fortunately, stochastic trace evaluation as initially proposed by Skilling [44] and later generalized by others [30, 45, 46] can be employed here. It consists of approximating the full trace $\text{Tr}(A)$ by $R \ll d$ randomly chosen quantum states. Using a set of R normalized states $|r\rangle$ whose complex coefficients are each drawn from a normal distribution we approximate traces by the average of the expectation values

$$\text{Tr}(O) = d \overline{\langle r | O | r \rangle} \quad (36)$$

where the overbar denotes the process of determining the arithmetic average over the R random states $\{|r\rangle\}$ and d is the dimension of the half-filled Hilbert space. The standard deviation of the estimate (36) scales like $1/\sqrt{Rd}$. Finally, inserting (36) and (29) into (30) leads to the approximated retarded Green's function

$$g(t) \approx -\frac{i}{R} \sum_{r=1}^R \langle r | e^{iH_{\text{eff}}t} \bar{h}_{i\uparrow} e^{-iH_{\text{eff}}t} \bar{h}_{i\uparrow}^\dagger | r \rangle \theta(t). \quad (37)$$

Below, we consider the hole dynamics in both the complete t - J model in its form H_{eff} as well as the hopping-only model $H_{0,\text{eff}}$. The last case, i.e., setting the magnetic exchange to zero with $J = 0$, allows for a significant simplification of (37) implying

$$g_{0,\text{eff}}(t) \approx -\frac{i}{R} \sum_{r=1}^R \langle r | \bar{h}_{i\uparrow} e^{-iH_{0,\text{eff}}t} \bar{h}_{i\uparrow}^\dagger | r \rangle \theta(t), \quad (38)$$

where we exploit that $e^{iH_{\text{eff}}t}$ for $J = 0$ has no impact on $\langle r |$ because no hopping can take place in $\langle r |$ such that this contribution in (37) can be omitted in (38).

The Green's functions (37) and (38) are calculated for a finite time span $[0; t_{\text{max}}]$ in time steps of dt . Thereafter, they are Fourier transformed

$$g(\omega) := \sum_n e^{-i\omega t_n} g(t_n) dt. \quad (39)$$

For the sake of notational brevity, we use the same symbol g for time and for frequency dependence.

The finite time interval leads to spurious phenomena in the Fourier transforms (39) which can be systematically suppressed by damping the temporal Green's function $g(t)$ by multiplying it with a decreasing function. For simplicity, we opt for the approach to damp the Green's function by means of

$$\tilde{g}(t) = g(t) \exp(-1/2 \cdot \sigma^2 t^2). \quad (40)$$

We recall that the multiplication in the time domain (40) is equal to the convolution of $g(\omega)$ in the frequency domain with the Gaussian kernel $K \propto \exp(-\omega^2/2\sigma^2)$. Finally, the spectral density of the single hole excitation is obtained by

$$A(\omega) = -\frac{1}{\pi} \text{Im} \tilde{g}(\omega). \quad (41)$$

To compute the Green's function, we need the time-dependence $|\psi(t)\rangle$ of the randomly chosen initial state after inserting the hole

$$|\psi(t)\rangle := \exp(-iHt) \bar{h}_{i\uparrow}^\dagger |r\rangle. \quad (42)$$

To do so we resort to the Chebyshev expansion technique [29] which consists of the expansion of the unitary time evolution operator $U(t) = \exp(-iH_{\text{eff}}t)$ in terms of Chebyshev polynomials

$$T_0(y) = 1, \quad T_1(y) = y \quad (43a)$$

$$T_{n+1}(y) = 2yT_n(y) - T_{n-1}(y) \quad (43b)$$

which are defined on the closed interval $I = [-1; 1]$. To be able to apply this technique to a general Hamiltonian H a finite rescaling $H \rightarrow H' = (H - b)/a$ is necessary to ensure that the spectrum of H' lies in the interval I . For this rescaling one needs an estimate of the extremal eigenvalues [42, 43, 47] of H to obtain $a = 1/2(E_{\text{max}} - E_{\text{min}})$ and $b = 1/2(E_{\text{max}} + E_{\text{min}})$. Note that estimates in the form of upper bounds for E_{max} and lower bounds for E_{min} are sufficient to warrant that the spectrum lies in I . Finally, the time-evolution operator becomes

$$U(t) = \sum_{n=0}^{\infty} \alpha_n(t) T_n(H') \quad (44a)$$

$$\alpha_n(t) = (2 - \delta_{n,0}) i^n e^{-ibt} J_n(at) \quad (44b)$$

where the time-dependence is embodied in the Bessel functions of the first kind $J_n(at)$. Eventually, the dynamics of an initial state $|\psi_0\rangle$ is given by

$$|\psi(t)\rangle = U(t) |\psi_0\rangle = \sum_{n=0}^{\infty} \alpha_n(t) \underbrace{T_n(H') |\psi_0\rangle}_{=: |\phi_n\rangle} \quad (45)$$

with the basis states of the expansion $|\phi_0\rangle = |\psi_0\rangle$ and $|\phi_1\rangle = H' |\psi_0\rangle$ as well as $|\phi_{n+1}\rangle = 2H' |\phi_n\rangle - |\phi_{n-1}\rangle$.

Numerically, the infinite series is cut off at some finite, but large value $N_c < \infty$. The time dependence of the prefactors resides in the Bessel functions $J_n(t)$ [48]. The higher the order n the longer the Bessel function $J_n(t)$ takes to contribute noticeably to the series. Hence, an estimate for the accuracy of the truncated series with cut-off N_c is given by

$$\epsilon \lesssim \left(\frac{at_{\max} \cdot e}{2N_c} \right)^{N_c}. \quad (46)$$

Consequently, the truncation error is not only related to N_c , but depends also on the maximum time up to which results are calculated as well as on the parameter a which equals half the width of the energy spectrum. An advantageous feature of the Chebyshev expansion is that increasing N_c linearly increases the time t_{\max} up to which the error estimate remains the same.

IV. REAL TIME DEPENDENCE AND BAND EDGES

A. Method comparison

In order to understand the two methods described in Sec. III better and to see their strengths and weaknesses we apply them to the full t - J model as given by Eq. (16) on the 1D chain with the parameters (A) in Eq. (17a). In all calculations, the hopping element t_0 defines the energy unit and the time unit according to $[t] = 1/t_0$.

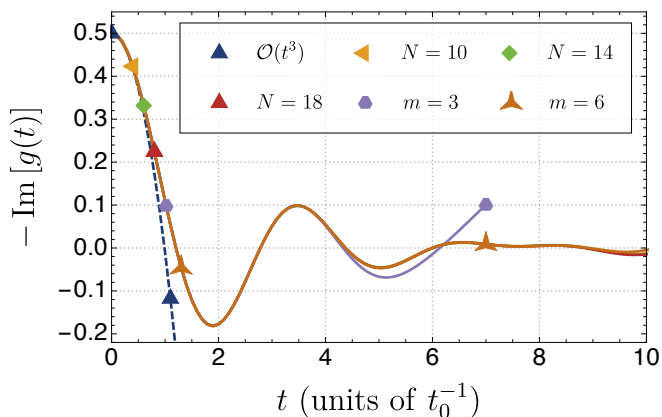


FIG. 2. Retarded Green's function of the 1D chain for the full t - J model with parameters (A) as given in Eq. (17a). Results are determined by (31) and (37) for various chain lengths N (CET) and loop orders m (iEoM). The parabola of the analytical expansion, cf. Appendix A, in powers of t up to $\mathcal{O}(t^3)$ is depicted as well (blue triangles). Note that the iEoM result for $m = 6$ loops first starts to deviate from the CET results at about $t \geq 9/t_0$.

Using (31) and (37), the results for the retarded Green's function $g(t)$ are presented in Fig. 2 for various chain lengths N (CET) and loop orders m (iEoM).

Furthermore, the short-time behavior of $g(t)$ is determined analytically by an expansion in powers of t , cf. Appendix A, and is plotted by a dashed line as reference. The Green's function starts at $g(t=0) = 0.5$ because the hole creation only works if an electron with the appropriate spin is present. Due to the assumed spin disorder this holds in 50% of the cases.

The time dependence in Fig. 2 resembles a damped oscillation. But since we are dealing with a closed quantum system no relaxation can occur, but the superposition of coherent oscillations is possible. In particular since we are dealing with a large mixture of spin backgrounds it is plausible that the damping stems from strong dephasing of very many eigenstates of the hole motion. In CET, no finite size effects appear in the studied time interval up to $t_{\max} = 20$ (not fully shown here) as supported by the coincidence of the results for $N = 10$, $N = 14$, and $N = 18$. A further analysis of finite size dependence is therefore not required and enables us to use simulations of the largest possible system sizes in subsequent computations by CET. The iEoM results agree very well with the CET results except for low loop order m . We emphasize that the iEoM dynamics consists of oscillatory contributions exclusively; no contributions to $g(t)$ decrease or increase exponentially due to the guaranteed unitarity of the dynamic matrix [27, 28].

For the calculations based on iEoM, we use the maximum available loop order m in the following. It varies and is strongly dependent on the topology of the lattice as well as on the number of physical processes considered. The number of processes depends on whether only first-order contributions in t_0/U with T_0 , second-order contributions without spin-spin interaction ($H_{0,\text{eff}}$), or the complete t - J model is considered. The numerically most challenging case is given by a high coordination number z in combination with the complete t - J model, i.e., for 2D and H_{eff} . For this case, we reached $m = 3$. Larger loop order are prohibited by the required memory.

B. Determination of band edges

A particularly interesting issue in the dynamics of a hole inserted into a disordered Mott insulator is the width of the Hubbard bands. In particular, we are interested in the lower band edge of the upper Hubbard band. In the particle-hole symmetric case this is equivalent to the upper band edge of the lower Hubbard band which reflects the hole motion. The necessary minimum energy eigenvalue ω_{\min} can be determined particularly advantageously and systematically from the iEoM results by extrapolating $\omega_{\min}(m)$ in the loop order $m \rightarrow \infty$. We emphasize that this procedure considers the translationally invariant infinite system for any value of m and takes larger and larger spatial range upon increasing m . Thus, for $m \rightarrow \infty$, the system corresponds to the entire lattice including all physically relevant processes. Because of the systematic nature of this

expansion and the absence of finite-size effects, the iEoM approach is particularly appropriate for the discussion of the band edges of the Hubbard bands and their supports. In return, we will see later that the CET yields a better access to the overall shape of the Hubbard bands.

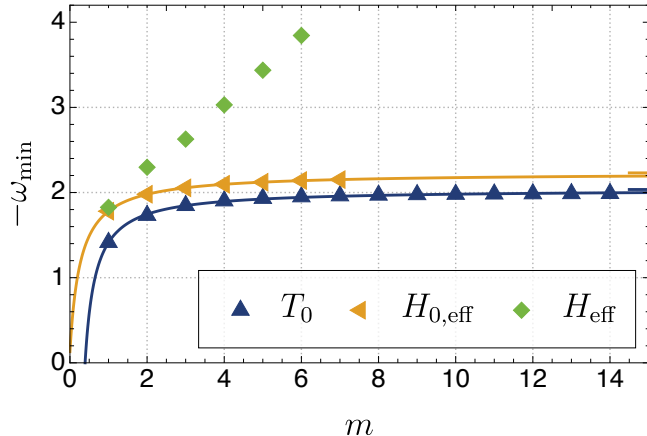


FIG. 3. Extrapolation of the minimum eigenvalue ω_{\min} for a one-dimensional chain and the parameters (A) in the loop order m of the iEoM. The minimum eigenvalues for the different loop orders are shown by symbols; solid lines mark fits of the form $-\omega_{\min}(m) = a/(m-b) + c$. The fit parameter $c = -\omega_{\min}(m \rightarrow \infty)$ is displayed using short horizontal bars at the right boundary of the graph.

The extrapolation is shown for the one-dimensional chain and parameters (A), cf. (17a); the results for parameters (B), cf. (17b), are qualitatively the same. Fig. 3 depicts the results. The different symbols mark the different cases depending on which processes are included in the Hamiltonian. The more processes are included in the Hamiltonian, the lower is the maximum achievable loop order m . If the minimum eigenvalues asymptotically converge towards a finite value

$$c := -\omega_{\min}(m \rightarrow \infty) \quad (47)$$

we determine this value by the fit

$$-\omega_{\min}(m) = \frac{a}{(m-b)} + c. \quad (48)$$

These fits are displayed by solid lines in Fig. 3; they describe the data shown by symbols very well. The asymptotic minimum eigenvalue c is marked by a horizontal bar at the right boundary of the graph. Several observations are in order. The more different couplings are included in the Hamiltonian the lower is the maximum loop order m . The key observation, however, is that there is no convergence if the magnetic exchange is included. As long as only hole hopping is considered, i.e., the Hamiltonian is T_0 or $H_{0,\text{eff}}$, clear convergence can be observed and the band edge can be determined reliably by fitting $-c$. If the magnetic exchange coupling is included, i.e., the Hamiltonian is H_{eff} , the convergence according to (48) is lost

and the band edge diverges linearly with m . This provides very strong evidence for an *unbounded* support of the corresponding spectral density of the Hubbard band.

This large qualitative difference comes as a surprise. But it can be understood by analyzing the magnetic degrees of freedom of the Mott insulating phase right at half-filling. This is an antiferromagnetic Heisenberg model with eigenenergies between the ground state energy $E_{\min} < 0$ and the maximum energy for fully polarized states $E_{\max} > 0$. Both energies are extensive, that means, they are proportional to the system size N implying that they are infinite in the thermodynamic limit. Thus, the disordered spin ensemble, which we consider as initial phase, can be expanded in eigenstates of which the eigenenergies range from minus to plus infinity. If a hole is inserted these eigenstates are disturbed locally at the site of the added hole. These disturbed states can again be expanded in eigenstates of the singly-doped t - J model. It is highly plausible that this expansion also consists of eigenstates with eigenenergies from minus to plus infinity. Hence, an unbounded support for the spectral density appears naturally.

We stress that the above qualitative argument does not *prove* that the support is unbounded, but it provides a plausible explanation for an unbounded support. One may object that the local disturbance by the added hole cannot change the energy by an infinite amount. But this argument only refers to the expectation value of the energy before and after the insertion of the hole. The above argument does not make statement on the matrix elements of the transitions so that a finite change of the energy expectation is perfectly consistent with the infinite support.

As an illustration that similar scenarios exist we refer to the example of spectral densities of local Green's functions of impurities in metallic hosts. Here the disturbance is also local, but the support of the spectral density is defined by all possible transitions from \mathbf{k} to \mathbf{k}' so that the support generically is as large as the full band width. We will come back to the shape of the spectral density of the hole motion in the disordered spin background below.

V. RESULTS FOR THE CHAIN

We consider explicit results for the local spectral densities and their lower band edge if it is finite. If no band edge exists we study the tails of the spectral densities.

A. Spectral densities

The spectral densities $A(\omega)$ for the one-dimensional chain for the three cases T_0 , $H_{0,\text{eff}}$, and H_{eff} are displayed in Figs. 4 and 5. For $H_{0,\text{eff}}$ and H_{eff} the difference of two parameter sets (A) and (B) matters. The results from the different methods used, CET (solid) and iEoM (dashed),

agree very well in all cases. Note that the data has been broadened by $\sigma = 0.15t_0$.

Both the upwards and the downwards flanks of the spectral density, as well as the characteristic shape including the peak positions are accurately reproduced. The wiggling of the iEoM results around $\omega = 0$ results from a few discrete, Gaussian broadened peaks. Higher loop order m and thus increased basis would lead to smoother spectral densities.

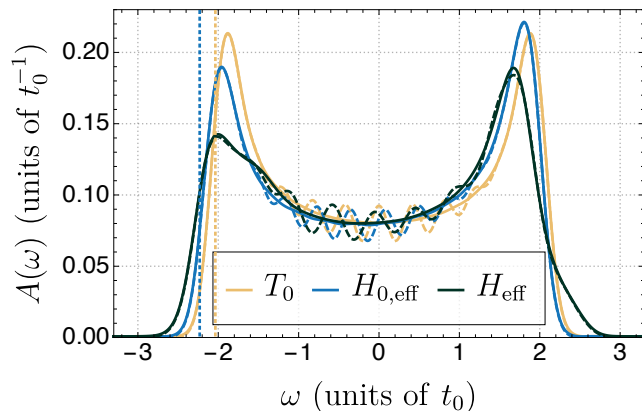


FIG. 4. Spectral density $A(\omega)$ vs. ω for a one-dimensional chain and the parameter set (A) in (17a), artificially broadened by $\sigma = 0.15t_0$. Solid lines represent CET results, dashed lines iEoM results. The band edges ω_{\min} determined from (47) are indicated by vertical dashed lines.

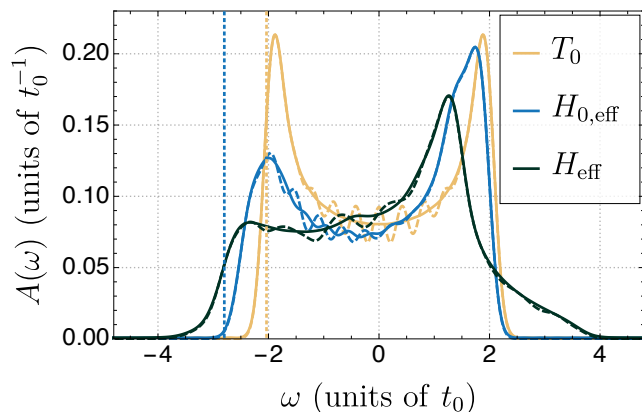


FIG. 5. Same as Fig. 4, but for the parameters (B) in (17b).

The spectral density $A(\omega)$ for T_0 is symmetric about $\omega = 0$. This is expected because it is obvious from T_0 that it corresponds to nearest-neighbor hopping which implies symmetric local densities-of-states (DOS). This has been shown rigorously in the 1D case in the limit $U \rightarrow \infty$ [5, 6]. This also explains the value of the lower band edge $\omega_{\min} = -2t_0$ which our extrapolation reproduces within a relative error of 2%. We emphasize that the determination of the band edges does not involve any broadening. The pronounced peaks are the van Hove singularities which are smeared out by finite-size effects or

finite loop order and the artificial broadening. Otherwise, they would show up as $1/\sqrt{\Delta\omega}$ divergences. In fact, the analytical results [5, 6] imply that the DOS is given by

$$A(\omega) = \frac{1}{2\pi} \frac{1}{\sqrt{\omega^2 - 4t_0^2}}. \quad (49)$$

If the spin-dependent and spin-independent hopping is included, i.e., we consider $H_{0,\text{eff}}$, the support of the spectrum increases. For parameter set (A) by about 10% and for set (B) by almost 20%. Since the DOS satisfies the sum rule $\int A(\omega) d\omega = 1/2$, a larger support necessarily translates into a reduced average height. In addition, one clearly sees that the DOS loses its symmetry: the left van Hove peak becomes lower than the right one. A physical explanation for this behavior is left to future research.

If the magnetic exchange, i.e., the spin-spin interaction, is included as well we consider the dynamics induced by H_{eff} . The corresponding data is shown by the darkest curves in Figs. 4 and 5. The broadened curves show a larger asymmetry between the left and the right peak compared to the curves for $H_{0,\text{eff}}$. For parameter set (B) the left peak is reduced to only a shoulder. In addition, it seems that the band edges have been slightly more shifted and broadened. But from the previous analysis of the non-convergence of the band edge we know that this impression is misleading. In fact, there is no finite support of the DOS anymore. We will analyze the tails of the DOS quantitatively in the next section.

B. Gaussian tails

In Sect. IV B we already found striking evidence that the spectral density differs qualitatively if the magnetic exchange is considered or not. Here we come back to this point and study the case with magnetic exchange, i.e., H_{eff} , in more detail. We want to find out what the tails of the spectral densities look like. Motivating starting point is the fact that the orientation of each spin at half-filling is chosen randomly and independently for each site in the completely disordered spin ensemble. Hence, an infinite number of independent random processes influences the matrix elements entering the spectral densities and their tails in particular. The central limit theorem suggests that the resulting tails are of Gaussians nature. This is consistent with the finding that the support of the spectral densities is infinite. But we emphasize that the hypothesis of Gaussian tails represents an educated guess at this stage. Therefore, we put this hypothesis to a quantitative test.

For this test we have to refrain from using any broadening because this induces artificial tails which conceal the intrinsic physics. Thus we do not consider the spectral density itself but its primitive as is routinely done in

probability theory. We define

$$f_-(\omega) = \int_{-\infty}^{\omega} A(x) dx \quad (50a)$$

$$f_+(\omega) = \int_{\omega}^{\infty} A(x) dx, \quad (50b)$$

where f_- is used to study the lower tail $\omega \rightarrow -\infty$ and f_+ for the upper tail $\omega \rightarrow \infty$. If the tails are Gaussian we have

$$f_-(\omega) \approx \frac{W_-}{\sqrt{2\pi}\sigma_-} \int_{-\infty}^{\omega} \exp(-(x-x_-)^2/(2\sigma_-^2)) dx \quad (51a)$$

$$= \frac{W_-}{2} (\text{erf}(\omega_-) + 1) \quad (51b)$$

$$f_+(\omega) \approx \frac{W_+}{\sqrt{2\pi}\sigma_+} \int_{\omega}^{\infty} \exp(-(x-x_+)^2/(2\sigma_+^2)) dx \quad (51c)$$

$$= \frac{W_+}{2} (1 - \text{erf}(\omega_+)), \quad (51d)$$

where

$$\omega_- := (\omega - x_-)/(\sqrt{2}\sigma_-) \quad (52a)$$

$$\omega_+ := (\omega - x_+)/(\sqrt{2}\sigma_+). \quad (52b)$$

Note that three free parameters need to be determined by fitting. Since exponentially small values occur we plot $\ln(f_{\pm})$ as function of $|\omega|$ in Fig. 6 and compare it with the fits (51). The best fit parameters are given in the caption. The corresponding results for the parameter set (B) can be found in Figs. 6 and 7.

The agreement between the data obtained by iEoM and the fits is very good. The logarithm of the iEoM data clearly shows roughly parabolic shape consistent with Gaussian tails. Of course, some fluctuations around the rigorous error functions occur. But we stress that the agreement found for all four fit extends over 15 (!) orders of magnitude if one converts the differences on the log-scale to decimal ratios. We take this observation as strong support for our claim of Gaussian tails.

The above finding of an infinite support of the DOS and of its Gaussian tails is in stark contrast to the findings of Ejima and co-workers [17] who studied the 1D Hubbard model by Bethe ansatz under the assumption of a completely disordered spin background. This appears indeed very similar to the physical situation studied in the present article. Ejima *et al.* determine a critical U_c below which the assumed Mott insulating phase becomes unstable. This implies that the Hubbard bands have finite, well-defined band edges which vanish if the shift by $U/2$ becomes to small. This is at variance with the above findings.

Two explanations for this difference are conceivable. First, Ejima *et al.* study the Hubbard model as such without prior mapping to the t - J model. This mapping certainly influences matrix elements and hence it will have a certain effect on the shape of the spectral density

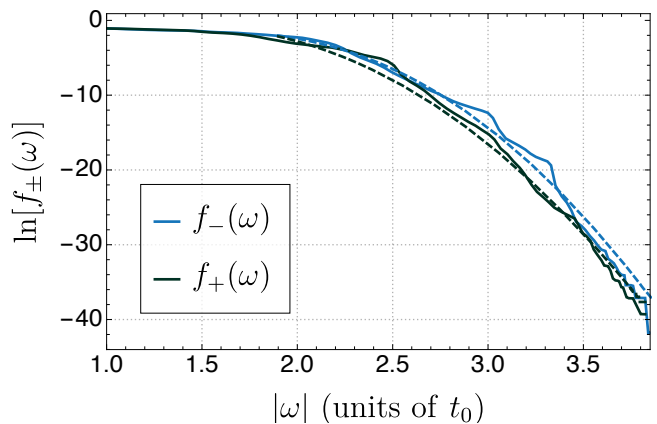


FIG. 6. Analysis of the lower and the upper tail of the spectral density as obtained by iEoM via the logarithm of the primitives defined in Eq. (50) for the parameter set (A). The primitives are shown as solid lines; the fits defined in Eq. (51) are shown as dashed lines. The optimum fit parameters read $W_- = 0.28$, $\sigma_- = 0.24t_0$, $x_- = -1.88t_0$ for the lower tail and $W_+ = 0.80$, $\sigma_+ = 0.26t_0$, $x_+ = 1.62t_0$ for the upper tail.

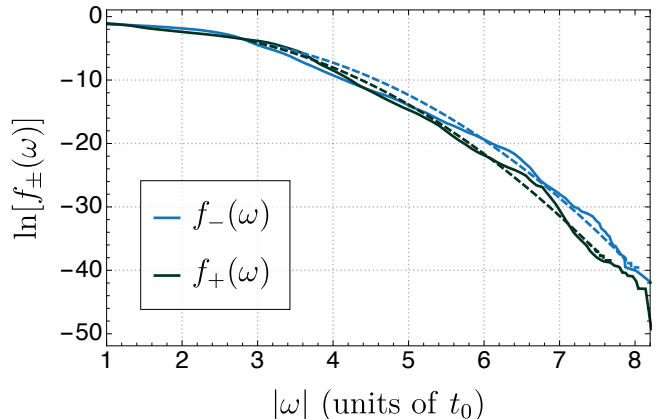


FIG. 7. Same as Fig. 6, but for parameters (B) and the fit parameters $W_- = 0.12$, $\sigma_- = 0.69t_0$, $x_- = -2.26t_0$ for the lower tail and $W_+ = 0.37$, $\sigma_+ = 0.70t_0$, $x_+ = 1.81t_0$ for the upper tail.

of hole motion. Yet, we think it is unlikely that this mapping changes a finite support to an infinite support, i.e., it is not plausible that matrix elements between eigenstates strongly differing in energy are induced by this mapping which are strictly zero in the Hubbard model itself. At present, however, we cannot exclude this explanation.

Second, the assumption of a totally disordered spin background is physically subtle. It is not difficult to construct the ensemble. But it must be kept in mind that it does not constitute a physically stable equilibrium situation except in the limit $J \ll T \ll t_0$ which represents an extreme parameter region with very large U (recall $J = 4t_0^2/U$). Hence, the occurrence of large energies in the spectral density of hole motion, induced by the large energy differences of the magnetic background in H_J , appears plausible. We presume that the energy differences

in the magnetic background are not included in the way the Bethe ansatz approach to hole hopping in disordered spins is conducted. But this interesting issue certainly calls for further elucidation.

The analyses in two dimensions analogous to the above analyses for the chain are not conclusive currently because of the limit loop order m that can be reached. But the preliminary results point into the same direction as in one dimension. In view of the conceptual interest of this issue a follow-up study should expand on this.

VI. RESULTS FOR THE SQUARE LATTICE

Analogous to calculations for the chain, spectral densities and band gaps can also be determined on the square lattice. We emphasize that such a calculation is not merely an enlargement of the dimension, but introduces additional physical processes. For instance, there are four nearest neighbors on a square lattice instead of two nearest neighbors on the chain yielding a more densely populated Hamiltonian matrix. In parallel, for the same tractable cluster size N , only \sqrt{N} hopping processes are available for NN hopping and correspondingly fewer for NNN or 3NN hopping until wrap-around effects occur in two dimensions. Thus, describing the dynamics without finite-size effects becomes immensely more demanding. As a result, the obtained densities are not as smooth as in one dimension and show more wiggling. The iEoM treats the thermodynamic limit by construction, but it cannot reach the same accuracy as in one dimension either because the additional physical processes reduce the maximum loop order m that can be reached.

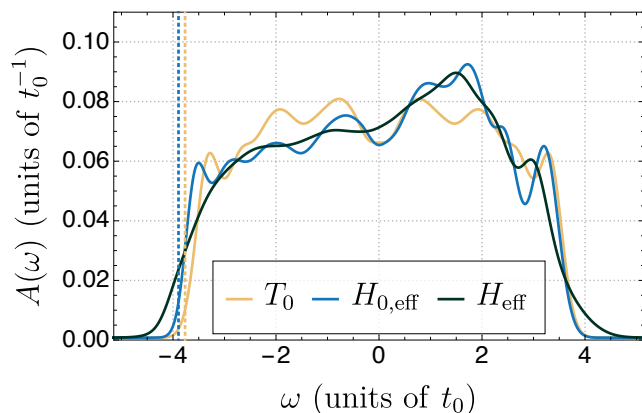


FIG. 8. Spectral density $A(\omega)$ for hole motion on the square lattice and parameter set (A). See caption of Fig. 4 for further explanations.

In order to achieve a higher number of hopping processes before wrap-around effects kick in, we resort to a trick and rotate the studied square cluster by 45° . Then its edge length is given by $\sqrt{2}n$ according to Pythagoras where n is the number of vertical and horizontal NN

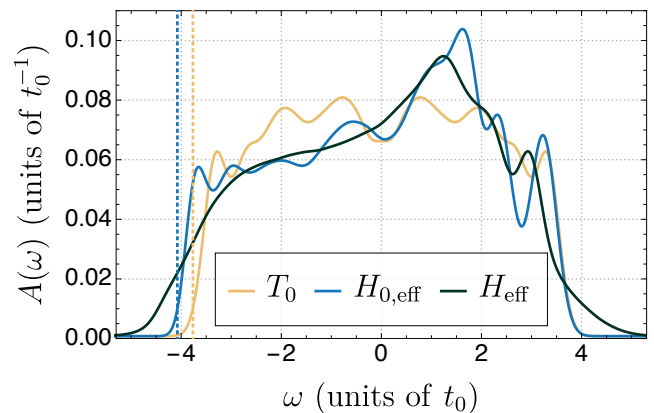


FIG. 9. Spectral density $A(\omega)$ for hole motion on the square lattice and parameter set (B). See caption of Fig. 4 for further explanations.

steps to pass from one corner of the square cluster to the adjacent one. Thus, the total number of sites is $N = 2n^2$. For $n = 3$ we have to treat 18 sites which is still feasible. The advantage is that a wrap-around only occurs after $2n = 6$ NN hops. We emphasize that a naive choice of the square cluster with an equal number of hops for wrap-around would have required $N = 6^2 = 36$ sites. The corresponding Hilbert space would be almost 2.6×10^5 times larger.

The overall shape of the spectrum is significantly altered compared to the case of a chain, see Figs. 8 and 9 for CET results. Results obtained by iEoM are presented and compared to CET results for larger broadening in Appendix B. In contrast to the two distinct van Hove singularities in the DOS the 2D case reveals a spectral density of approximately elliptical to rectangular shape. It is symmetric if only T_0 is considered and becomes asymmetric as soon as the Hamiltonian is extended in agreement with what we found in one dimension. Note, however, that the lower band edge for T_0 is not $-4t_0$, but in its vicinity (see vertical dashed lines in Figs. 8 and 9), as one would have expected for simple NN hopping in contrast to the 1D case where we found $-2t_0$ in accordance with analytical arguments [5, 6]. The reason is that in 1D at $U = \infty$ perfect spin-charge separation for NN hopping occurs, i.e., the sequence of spins is not changed at all by the hole motion. On the square lattice, this is no longer true since loops occur and only Trugman paths [2] allow for hole motion without changes of the spin order.

For the square lattice, the semi-analytically determined band edges ω_{\min} are significantly closer to each other for the two cases displayed than for the one-dimensional case. For the parameter set (A) we attribute this to the altered dimensionality. For parameter set (B), this effect is enhanced by the smaller value of the exchange coupling J , i.e. because of $J_{1D,B} = 1 > 1/2 = J_{2D,B}$. We emphasize that our results agree with results of previous research, for instance $\omega_c = -4.4t_0$ for the full

t - J model as given in Ref. [25]. This is in the range of the left flanks where the DOS starts rising significantly, cf. black curves in Figs. 8 and 9. An exact determination of the band edge is not possible due to the previously motivated Gaussian tails. We stress that this finding is not an artefact of the iEoM technique, but reflects the underlying physics.

Analogous to the one-dimensional case, a broadening of the spectrum upon including more and more processes is observed on the square lattice. For parameter set (A) the spectrum broadens from T_0 to the complete t - J model H_{eff} by about 13%; for parameter set (B) by almost 25%. Instead of peaks at the boundaries of the DOS one observes knee-like flanks.

VII. SUMMARY AND CONCLUSIONS

In this work, we studied the dynamics of single hole in a disordered spin background for the t - J model as it results for the Mott insulating phase from the Fermi-Hubbard model by an expansion in t_0/U where U is the local repulsion and t_0 the nearest-neighbor (NN) hopping. For this purpose, we systematically extended the NN hopping T_0 via spin-dependent and spin-independent NNN and 3NN hopping to the full t - J model including the spin-spin exchange interaction $\mathbf{S}_i\mathbf{S}_j$. For the one-dimensional chain and the two-dimensional square lattice we computed the lower band edges of the Hubbard bands and the shape of the local spectral density, i.e., the density-of-states (DOS). This is achieved by two approaches, the iterated equations of motion (iEoM) and the Chebyshev expansion technique (CET).

The CET is a well-established numerically exact method for the analysis of finite clusters whose effort increases exponentially with the Hilbert space size. The iEoM addresses the infinite translationally invariant lattice, i.e., the thermodynamic limit. The systematic enlargement of the iEoM to processes of larger and larger spatial range by increasing the loop order m renders pro-

found statements on the existence and the value of well-defined band edges possible. We found strong evidence that the support of the DOS is only finite if hole hoppings enter the Hamiltonian exclusively. Once magnetic exchange is switched on the support becomes infinite and the DOS develops Gaussian tails. This effect has not yet been observed or discussed in the literature to our knowledge. In contrast, a previous analysis of the Hubbard model based on Bethe ansatz found finite band edges for the hole motion in a disordered spin background [17]. At present, it is unclear whether this difference results from the study of the different, though related models, Fermi-Hubbard model and t - J model, or from differences in the treatment of the magnetic dynamics and surely merits further investigation.

Our analysis has become possible by the use of the iEoM. The evidence for Gaussian tails is rather stringent in one dimension, but indications for Gaussian tails exist as well in two dimensions. The substantially higher numerical effort in two dimensions calls for further efforts to corroborate the advocated scenario further. Analogous studies for other lattices in two dimensions and also in three dimensions to study the influence of lattice topology are conceivable and desirable.

ACKNOWLEDGMENTS

We gratefully acknowledge financial support by the Konrad Adenauer Foundation (PB) as well as by the German Research Foundation (DFG) in projects UH 90-13/1 (GSU) and UH 90-14/1 (DBH) as well as in project B9 of ICRC 160 (GSU) together with the Russian Foundation for Basic Research. All authors contributed equally to this work, PB and GSU wrote the manuscript. The authors are indebted to Florian Gebhard for helpful and fruitful discussions.

-
- [1] F. Gebhard, *The Mott Metal-Insulator Transition*, Springer Tracts in Modern Physics, Vol. 137 (Springer, Berlin, 1997).
 - [2] S. A. Trugman, Interaction of holes in a Hubbard antiferromagnet and high-temperature superconductivity, *Phys. Rev. B* **37**, 1597 (1988).
 - [3] J. Bonča, S. Maekawa, and T. Tohyama, Numerical approach to the low-doping regime of the t - J model, *Phys. Rev. B* **76**, 035121 (2007).
 - [4] M. Mierzejewski, L. Vidmar, J. Bonča, and P. Prelovšek, Nonequilibrium quantum dynamics of a charge carrier doped into a Mott insulator, *Phys. Rev. Lett.* **106**, 196401 (2011).
 - [5] A. Mielke, The one-dimensional Hubbard model for large or infinite U , *J. Stat. Phys.* **62**, 509 (1991).
 - [6] B. Kumar, Exact solution of the infinite- U Hubbard problem and other models in one dimension, *Phys. Rev. B* **79**, 155121 (2009).
 - [7] A. Nocera, F. H. Essler, and A. E. Feiguin, Finite-temperature dynamics of the Mott insulating Hubbard chain, *Phys. Rev. B* **97**, 1 (2018).
 - [8] M. P. Eastwood, F. Gebhard, E. Kalinowski, S. Nishimoto, and R. M. Noack, Analytical and numerical treatment of the Mott-Hubbard insulator in infinite dimensions, *Eur. Phys. J. B* **35**, 155 (2003).
 - [9] S. Nishimoto, F. Gebhard, and E. Jeckelmann, Dynamical density-matrix renormalization group for the Mott-Hubbard insulator in high dimensions, *J. Phys. Condens. Matter* **16**, 7063 (2004).
 - [10] R. Bulla, Zero temperature metal-insulator transition in

- the infinite-dimensional Hubbard model, Phys. Rev. Lett. **83**, 136 (1999).
- [11] R. Bulla, T. A. Costi, and D. Vollhardt, Finite temperature numerical renormalization group study of the Mott transition, Phys. Rev. B **64**, 045103 (2001).
- [12] D. J. Garcia, K. Hallberg, and M. J. Rozenberg, Dynamical mean field theory with the density matrix renormalization group, Phys. Rev. Lett. **93**, 246403 (2004).
- [13] N. Blümer and E. Kalinowski, The Mott insulator: Tenth-order perturbation theory extended to infinite order using a quantum Monte Carlo, Phys. Rev. B **71**, 195102 (2005).
- [14] M. Karski, C. Raas, and G. S. Uhrig, Electron spectra close to a metal-to-insulator transition, Phys. Rev. B **72**, 113110 (2005).
- [15] M. Karski, C. Raas, and G. S. Uhrig, Single-particle dynamics in the vicinity of the Mott-Hubbard metal-to-insulator transition, Phys. Rev. B **77**, 075116 (2008).
- [16] F. H. L. Essler, H. Frahm, F. Göhmann, A. Klümper, and V. E. Korepin, *The One-Dimensional Hubbard Model* (Cambridge University Press, Cambridge, United Kingdom, 2005).
- [17] S. Ejima, F. H. Essler, and F. Gebhard, Thermodynamics of the one-dimensional half-filled Hubbard model in the spin-disordered regime, J. Phys. A: Math. Gen. **39**, 4845 (2006).
- [18] P. W. Anderson, New approach to the theory of superexchange interactions, Phys. Rev. **115**, 2 (1959).
- [19] A. B. Harris and R. V. Lange, Single-particle excitations in narrow energy bands, Phys. Rev. **157**, 295 (1967).
- [20] D. J. Klein and W. A. Seitz, Perturbation expansion of the linear Hubbard model, Phys. Rev. B **8**, 2236 (1973).
- [21] M. Takahashi, Half-filled Hubbard model at low temperature, J. Phys. C **10**, 1289 (1977).
- [22] A. H. MacDonald, S. M. Girvin, and D. Yoshioka, t/U expansion for the Hubbard model, Phys. Rev. B **37**, 9753 (1988).
- [23] J. Stein, Flow equations and the strong-coupling expansion for the Hubbard model, J. Stat. Phys. **88**, 487 (1997).
- [24] H. Eskes, A. M. Oleś, M. B. J. Meinders, and W. Stephan, Spectral properties of the Hubbard bands, Phys. Rev. B **50**, 17980 (1994).
- [25] A. Reischl, E. Müller-Hartmann, and G. S. Uhrig, Systematic mapping of the Hubbard model to the generalized t - J model, Phys. Rev. B **70**, 1 (2004).
- [26] S. A. Hamerla, S. Duffe, and G. S. Uhrig, Derivation of the t - J model for finite doping, Phys. Rev. B **82**, 235117 (2010).
- [27] M. Kalthoff, F. Keim, H. Krull, and G. S. Uhrig, Comparison of the iterated equation of motion approach and the density matrix formalism for the quantum Rabi model, Eur. Phys. J. B **90**, 97 (2017).
- [28] P. Bleicker and G. S. Uhrig, Strong quenches in the one-dimensional Fermi-Hubbard model, Phys. Rev. A **98**, 033602 (2018).
- [29] H. Tal-Ezer and R. Kosloff, An accurate and efficient scheme for propagating the time dependent Schrödinger equation, J. Chem. Phys. **81**, 3967 (1984).
- [30] A. Weiße, G. Wellein, A. Alvermann, and H. Fehske, The kernel polynomial method, Rev. Mod. Phys. **78**, 275 (2006).
- [31] P. Bleicker, J. Stolze, and G. S. Uhrig, Probing thermalization in quenched integrable and nonintegrable Fermi-Hubbard models, Phys. Rev. A **102**, 1 (2020).
- [32] J. Hubbard, Electron Correlations in Narrow Energy Bands, Proc. R. Soc. A Math. Phys. Eng. Sci. **276**, 238 (1963).
- [33] J. Kanamori, Electron Correlation and Ferromagnetism of Transition Metals, Prog. Theor. Phys. **30**, 275 (1963).
- [34] M. C. Gutzwiller, Effect of Correlation on the Ferromagnetism of Transition Metals, Phys. Rev. **134**, A923 (1964).
- [35] F. Wegner, Flow-equations for Hamiltonians, Ann. Phys. **506**, 77 (1994).
- [36] A. Mielke, Flow equations for band-matrices, Eur. Phys. J. B **5**, 605 (1998).
- [37] C. Knetter and G. S. Uhrig, Perturbation theory by flow equations: dimerized and frustrated $s = 1/2$ chain, Eur. Phys. J. B **13**, 209 (2000).
- [38] S. Kehrein, *The Flow Equation Approach to Many-Particle Systems*, Springer Tracts in Modern Physics, Vol. 217 (Springer, Berlin, 2006).
- [39] G. S. Uhrig, Interaction quenches of Fermi gases, Phys. Rev. A **80**, 061602 (2009).
- [40] S. A. Hamerla and G. S. Uhrig, Dynamical transition in interaction quenches of the one-dimensional Hubbard model, Phys. Rev. B **87**, 064304 (2013).
- [41] S. A. Hamerla and G. S. Uhrig, Interaction quenches in the two-dimensional fermionic Hubbard model, Phys. Rev. B **89**, 104301 (2014).
- [42] W. E. Arnoldi, The principle of minimized iteration in the solution of the matrix eigenvalue problem, Q. Appl. Math. **9**, 17 (1951).
- [43] C. Lanczos, An iteration method for the solution of the eigenvalue problem of linear differential and integral operators, J. Res. Natl. Bur. Stand. (1934). **45**, 255 (1950).
- [44] J. Skilling, *Maximum Entropy and Bayesian Methods*, edited by J. Skilling (Springer Netherlands, Dordrecht, 1988) pp. 455–466.
- [45] D. A. Drabold and O. F. Sankey, Maximum entropy approach for linear scaling in the electronic structure problem, Phys. Rev. Lett. **70**, 3631 (1993).
- [46] R. Silver and H. Röder, Densities of states of megadimensional Hamiltonian matrices, Int. J. Mod. Phys. C **05**, 735 (1994).
- [47] J. Kuczyński and H. Woźniakowski, Estimating the Largest Eigenvalue by the Power and Lanczos Algorithms with a Random Start, SIAM J. Matrix Anal. Appl. **13**, 1094 (1992).
- [48] F. W. J. Olver, A. B. O. Daalhuis, D. W. Lozier, B. I. Schneider, R. F. Boisvert, C. W. Clark, B. R. Miller, and B. V. Saunders, eds., *Digital Library of Mathematical Functions* (NIST, 2019) p. Release 1.0.23.

Appendix A: Approximation of the short-time behavior of $g(t)$

The behavior of the retarded Green's function $g(t)$ for $t \gtrsim 0$ can be estimated analytically by an expansion in powers of t . The result reads

$$g(t) \approx -\frac{i}{2} \left(1 + \left\langle \left[H, \bar{h}_{i,\uparrow}(0) \right] \left[H, \bar{h}_{i,\uparrow}^\dagger(0) \right] \right\rangle t^2 \right) + \mathcal{O}(t^3) \quad (\text{A1})$$

where the translational invariance in time, i.e.,

$$g'(t) = g'(-t) = \left\langle \left[H, \bar{h}_{i,\uparrow}(0) \right] \bar{h}_{i,\uparrow}^\dagger(-t) \right\rangle \quad (\text{A2})$$

allows us to apply the second derivative to the second operator

$$g''(t) = \frac{dg'(-t)}{dt} = -i \left\langle \left[H, \bar{h}_{i,\uparrow}(0) \right] \left[H, \bar{h}_{i,\uparrow}^\dagger(0) \right] \right\rangle. \quad (\text{A3})$$

In this way, a double commutator is avoided.

For clarity, we apply formula (A1) to the one-dimensional chain. The commutators appearing are

$$\left[T_0, \bar{h}_{i,\uparrow} \right] = t_0 \bar{h}_{i\pm 1, \downarrow} \sigma_i^+ + \frac{1}{2} t_0 \bar{h}_{i\pm 1, \uparrow} \sigma_i^z + \frac{1}{2} t_0 \bar{h}_{i\pm 1, \uparrow} \quad (\text{A4a})$$

$$\left[T_0'', \bar{h}_{i,\uparrow} \right] = t'' \bar{h}_{i\pm 2, \downarrow} \sigma_i^+ + \frac{1}{2} t'' \bar{h}_{i\pm 2, \uparrow} \sigma_i^z + \frac{1}{2} t'' \bar{h}_{i\pm 2, \uparrow} \quad (\text{A4b})$$

$$\left[T_{s,0}'', \bar{h}_{i,\uparrow} \right] = \frac{1}{2} t_s'' \bar{h}_{i\pm 2, \downarrow} \sigma_{i\pm 1}^+ + \frac{1}{2} t_s'' \bar{h}_{i\pm 2, \downarrow} \sigma_{i\pm 1}^z \quad (\text{A4c})$$

$$+ t_s'' \bar{h}_{i\pm 2, \uparrow} \sigma_{i\pm 1}^- + \frac{1}{4} t_s'' \bar{h}_{i\pm 2, \uparrow} \sigma_{i\pm 1}^z \quad (\text{A4d})$$

$$+ \frac{1}{4} t_s'' \bar{h}_{i\pm 2, \uparrow} \sigma_{i\pm 1}^z - \frac{1}{2} t_s'' \bar{h}_{i\pm 2, \downarrow} \sigma_{i\pm 1}^z \sigma_i^+ \quad (\text{A4e})$$

$$\left[H_J, \bar{h}_{i,\uparrow} \right] = \frac{1}{4} J \bar{h}_{i,\uparrow} \sigma_{i\pm 1}^z + \frac{1}{2} \bar{h}_{i,\downarrow} \sigma_{i\pm 1}^+. \quad (\text{A4f})$$

The remaining commutators for the case $\bar{h}_{i,\uparrow}^\dagger$ result from the relations (A4) substituting $\bar{h}_{i,\uparrow} \rightarrow -\bar{h}_{i,\uparrow}^\dagger$ as well as $\sigma^+ \leftrightarrow \sigma^-$. The expectation values occurring in (A1) can be calculated straightforwardly since they are to be determined at $t = 0$. The trace is computed over states at half-filling without a hole. For demonstration purposes, we give the results for the expectation values that arise from H_J , see (A4f),

$$\left\langle \bar{h}_{i,\uparrow} \sigma_{i\pm 1}^z \bar{h}_{i,\uparrow}^\dagger \sigma_{i\pm 1}^z \right\rangle = 2 \cdot \frac{1}{2} \quad (\text{A5a})$$

$$\left\langle \bar{h}_{i,\downarrow} \sigma_{i\pm 1}^+ \bar{h}_{i,\downarrow}^\dagger \sigma_{i\pm 1}^- \right\rangle = 2 \cdot \frac{1}{4}. \quad (\text{A5b})$$

Here, the first factor results from the double occurrence of the expectation value, once for $i+1$ and once for $i-1$. The expectation values from the other contributions can be calculated similarly. Substituting all expectation values and (A4) into (A1) then yields the explicit expansion

$$g(t) = -\frac{i}{2} \left[1 - \left(t_0^2 + t''^2 + \frac{6}{16} t_s''^2 + \frac{3}{32} J^2 \right) t^2 \right] + \mathcal{O}(t^3). \quad (\text{A6})$$

Appendix B: 2D results from iEoM and CET

In addition to the results obtained for the square lattice using CET, convolved with $\sigma = 0.15t_0$, and shown in

Figs. 8 and 9, the analogous results can also be obtained using iEoM. Due to the limited loop order m they need to be broadened more strongly by Gaussians.

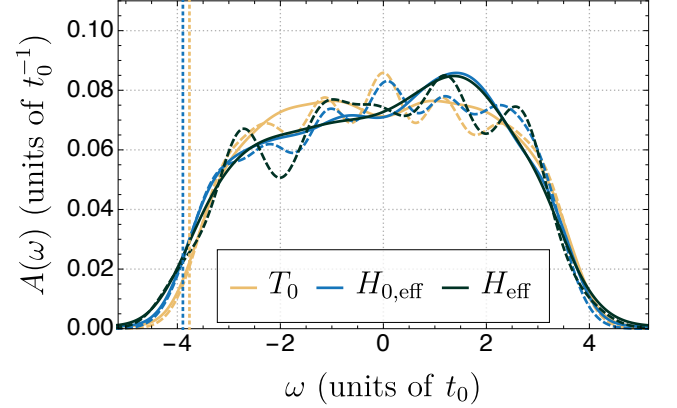


FIG. 10. Spectral densities $A(\omega)$ for the square lattice, parameter set (A), and the various contributions, calculated with CET for $N = 18$ (solid) and iEoM for $m = 4$ for T_0 and $H_{0,\text{eff}}$ and $m = 3$ for H_{eff} (dashed). All data are convolved with $\sigma = 0.45t_0$. The band edges ω_{min} calculated according to (47) are indicated by vertical dashed lines.

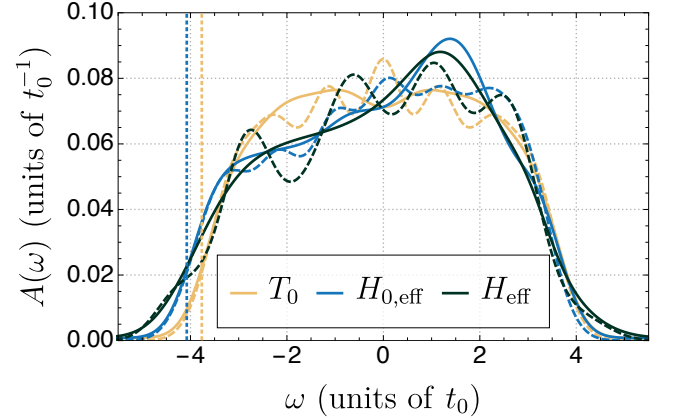


FIG. 11. Same as in Fig. 10, but for parameter set (B).

In view of the fact that the maximum possible loop order m is comparatively limited, wiggly spectral densities occur. In order to ensure a reasonable comparability to CET results and showing the good agreement of both methods a convolution of (all) results with an increased $\sigma = 0.45t_0$ is performed. Still, the iEoM results display some spurious wiggles. The corresponding results for the sets (A) and (B) are depicted in Figs. 10 and 11. The increased width of the CET results compared to the ones in Figs. 8 and 9 is an artefact due to the enhanced broadening. Obviously, the band edges obtained from the minimum eigenvalues of the Liouville matrix in iEoM are identical regardless of the additional broadening.

The high degree of agreement between the two methods in the margins of the spectral density can be understood in particular on the basis of the fact that the

Lanczos algorithm used is particularly accurate in the range of extremal eigenvalues. Increasing Krylov space

dimensions f as well as an increase of the loop order m lead to an even higher similarity of the results of both methods.